# *Electronic Supplementary Information*

# *for*

## Photochromic reaction in 3*H*-naphthopyrans studied by vibrational spectroscopy and quantum chemical calculations

Sabina Brazevic,[a] Stanislaw Nizinski,[a] Rafał Szabla,[b] Michał F. Rode*[b] and Gotard Burdzinski*[a]

[a] Quantum Electronics Laboratory, Faculty of Physics,

Adam Mickiewicz University in Poznan, Umultowska 85, 61-614 Poznan, Poland

E-mail: gotardb@amu.edu.pl

[b] Institute of Physics, Polish Academy of Sciences, Aleja Lotnikow 32/46, 02-668 Warsaw, Poland.

E-mail: mrode@ifpan.edu.pl

# OUTLINE

**Two types of conical intersections present in the TC-u↔TT-u photoisomerization process $CI_2(S_1/S_0)$ and $CI_3(S_1/S_0)$**

As the $S_1 \rightarrow S_0$ emission pathway is minor, practically the whole energy of photoexcitation should be dissipated into heat due to fast nonradiative channels associated with nonadiabatic transition at the multiple CI regions.

The **$CI_3(S_1/S_0)$** conical intersection responsible for the photoisomerization between the two forms can be readily found when the optimization procedure is started from the Franck-Condon region of the **TT-u** isomer. The $\delta(C_5\text{-}C_{14}\text{=}C_1\text{-}C_2)$ dihedral angle, identified above as the driving coordinate for the **TT-u↔TC-u** photoisomerization, amounts to -115.9º and the distance between the $C_{14}$ and $C_1$ atoms is equal to 1.48 Å. In addition, this **$CI_3$** geometry is characterized by the $C_2\text{=}C_3$ bond elongated up to 1.44 Å and a modest rotation of the phenyl substituents around this bond by approximately 20.0º. These nuclear parameters suggest that the photochemical interconversion between the **TC-u** and **TT-u** isomers might resemble the bicycle pedal photoisomerization mechanism reported for the first time by Warshel.[1-3] The bicycle-pedal mechanism would be here described as the twist about the two double bonds: $C_1\text{=}C_{14}$ and $C_2\text{=}C_3$ in opposing directions so that the two phenyl rings would remain in a similar orientation with respect to the naphthalenone moiety during the photoisomerization process. This mechanism might be in fact favorable in solution phase, where the rotation occurring solely around the $C_1\text{=}C_{14}$ bond would be hindered by significant friction around the phenyl substituents. This friction would be otherwise reduced by the bicycle-pedal photoisomerization mechanism. It is also worth noting that the **TT-u↔TC-u** photoisomerization is available after the photoexcitation of both of the involved isomers and it could occur on a sub-picosecond timescale owing to the peaked topography of the **$CI_3(S_1/S_0)$** state crossing.

Apart from the conical intersection responsible for the photochemical **TT-u↔TC-u** interconversion, we also identified the **$CI_2(S_1/S_0)$** conical intersection (the geometry of both **$CI_2$** and **$CI_3$** are given in Table S7) that is available exclusively from the **TC-u** form. Unlike the **$CI_3(S_1/S_0)$** state crossing, the **$CI_2(S_1/S_0)$** conical intersection is characterized by only slight rotation about the $C_1\text{=}C_{14}$ and $C_2\text{=}C_3$ bonds of approximately 20º (see $B_F$-N dihedral angle in Table S7) in both cases. The $C_1\text{=}C_{14}$ and $C_2\text{=}C_3$ bond lengths are virtually identical for both these conical intersection geometries, i.e. 1.48 Å and 1.44 Å respectively. However, given the very modest displacement of the $\delta(C_5\text{-}C_{14}\text{=}C_1\text{-}C_2)$ dihedral angle the **$CI_2(S_1/S_0)$** conical intersection does not allow for the population of the **TT-u** form. Therefore, the **$CI_2(S_1/S_0)$** state crossing enables efficient repopulation of the **TC-u** electronic ground state and is a photostabilizing channel for this isomer. The presence of this photostabilizing conical intersection could also explain the relatively low **TT-u** to **TC-u** ratio in the photoproduct mixture just after switching off UV irradiation.

**Table S1**. The adiabatic energy of the given form (in *eV*) relative to the closed global minimum form, **CF**, calculated at the different theory level.

| Method/Structure | MP2/cc-pVDZ | MP2/cc-pVTZ | MP2/aug-cc-pVDZ |
|---|---|---|---|
| **CF** | 0.00 | 0.00 | 0.00 |
| **TC-d** | 0.84 | 0.91 | 0.85 |
| **TC-u** | 0.59 | 0.66 | 0.70 |
| **TT-u** | 0.62 | 0.69 | 0.72 |
| **TT-d** | 0.64 | 0.67 | 0.49 |
| **AP** | 1.02 | 1.08 | 1.03 |

**Table S2.** Vertical excitation energy ($\Delta E^{VE}$, in eV and $\lambda_{abs}$, in nm calculated *vs*. experimental), oscillator strength (*f*), and dipole moment ($\mu_e$, in Debye) of the lowest singlet states for the equilibrium forms of the **NP** molecule calculated with the **CC2/aug-cc-pVDZ** method at the ground state geometries optimized at the **MP2/cc-pVDZ** theory level.

| $S_0$ form | | $\Delta E^{VE}$ calc. | $\lambda_{abs}$ calc. | *f* calc. | $\mu_e$ calc. | $\Delta E^{VE}$ expt. | $\lambda_{abs}$ expt. |
|---|---|---|---|---|---|---|---|
| **CF** | $S_0$ | *0.0* | | - | *0.9* | | |
| | $S_0 \rightarrow S_1 (\pi\pi^*)$ | 3.70 | 335 nm | 0.081 | 1.0 | 3.47 eV | 361 nm |
| | $S_0 \rightarrow S_2 (\pi\pi^*)$ | 4.23 | 293 nm | 0.084 | 1.7 | | |
| | $S_0 \rightarrow S_3 (n\pi^*)$ | 4.60 | | 0.004 | 3.3 | | |
| | $S_0 \rightarrow S_4 (n\pi^*)$ | 4.84 | | 0.007 | 7.1 | | |
| | | | | | | | |
| **TC-u** | $S_0$ | *0.59*[a] | | - | *2.8* | | |
| | $S_0 \rightarrow S_1 (n\pi^*)$ | 2.71 | 458 nm | 0.031 | 1.3 | | |
| | $S_0 \rightarrow S_2 (\pi\pi^*)$ | 2.97 | 418 nm | 0.714 | 5.5 | 2.91 | 427 nm |
| | $S_0 \rightarrow S_3 (\pi\pi^*)$ | 3.52 | 353 nm | 0.091 | 8.4 | | |
| | $S_0 \rightarrow S_4 (\pi\pi^*)$ | 4.15 | | 0.143 | 5.5 | | |
| | | | | | | | |
| **TC-d** | $S_0$ | *0.84*[a] | | - | *1.5* | | |
| | $S_0 \rightarrow S_1 (\pi\pi^*)$ | 2.47 | 502 nm | 0.115 | 0.6 | | |
| | $S_0 \rightarrow S_2 (\pi\pi^*)$ | 3.14 | 395 nm | 0.366 | 3.6 | | |
| | $S_0 \rightarrow S_3 (\pi\pi^*)$ | 3.49 | 356 nm | 0.031 | 7.8 | | |
| | $S_0 \rightarrow S_4 (\pi\pi^*)$ | 4.01 | | 0.028 | 3.3 | | |
| | | | | | | | |
| **TT-u** | $S_0$ | *0.62*[a] | | - | *3.0* | | |
| | $S_0 \rightarrow S_1 (\pi\pi^*)$ | 2.81 | 441 nm | 0.110 | 0.8 | | |
| | $S_0 \rightarrow S_2 (\pi\pi^*)$ | 3.08 | 403 nm | 0.600 | 6.0 | 3.03 | 409 nm |
| | $S_0 \rightarrow S_3 (\pi\pi^*)$ | 3.63 | 342 nm | 0.052 | 7.5 | | |
| | $S_0 \rightarrow S_4 (\pi\pi^*)$ | 4.20 | 295 nm | 0.149 | 4.7 | | |
| | $S_0 \rightarrow S_5 (\pi\pi^*)$ | 4.35 | 285 nm | 0.098 | | | |
| | | | | | | | |
| **TT-d** | $S_0$ | *0.64*[a] | | - | *4.2* | | |
| | $S_0 \rightarrow S_1 (\pi\pi^*)$ | 2.82 | 440 nm | 0.051 | 2.0 | | |
| | $S_0 \rightarrow S_2 (\pi\pi^*)$ | 3.03 | 409 nm | 0.172 | 7.3 | | |
| | $S_0 \rightarrow S_3 (\pi\pi^*)$ | 3.53 | 351 nm | 0.028 | 7.1 | | |
| | $S_0 \rightarrow S_4 (\pi\pi^*)$ | 3.82 | 325 nm | 0.034 | 8.5 | | |
| | $S_0 \rightarrow S_5 (\pi\pi^*)$ | 4.15 | 299 nm | 0.030 | 4.5 | | |
| | | | | | | | |
| **AP** | $S_0$ | *1.02*[a] | | | 1.4 | | |
| | $S_0 \rightarrow S_1 (\pi\pi^*)$ | 3.86 | 321 nm | 0.148 | 2.0 | | below 400 nm |
| | $S_0 \rightarrow S_2 (\pi\pi^*)$ | 4.14 | 300 nm | 0.039 | 11.0 | | |
| | $S_0 \rightarrow S_3 (\pi\pi^*)$ | 4.42 | 281 nm | 0.193 | 1.0 | | |
| | $S_0 \rightarrow S_4 (\pi\pi$ | 4.64 | 267 nm | 0.005 | 10.0 | | |

[a] adiabatic energy of the given ($E_a$, in eV) form relative to the closed form, **CF**, calculated at the MP2/cc-pVDZ theory level.

***** mean error of calculated $\Delta E^{VE}$ is below 0.3 eV [4-6]

**Table S3.** The spectral position ($cm^{-1}$) of vibrational C=O stretching mode of **TC-u** and **TT-u** isomers of **NP** in different solvents.

| Solvent | ν, $cm^{-1}$ | |
|---|---|---|
| | **TC-u** | **TT-u** |
| Cyclohexane | 1644 | 1655 |
| Acetonitrile-$d_3$ | 1638 | 1647 |
| Methanol-OD | 1630 | 1641 |

**Table S4.** Comparison of the geometric parameters (bond lengths, in Å), adiabatic energies ($E_a$, in eV) for the ground state ($S_0$) geometries optimized at the **MP2/cc-pVDZ** level of theory. $B_F$-N denotes phenyl- naphthalenone dihedral angle, BB corresponds to phenyl-phenyl dihedral angle.

| | R $C_3$-$O_4$ [Å] | δ $C_5$-$C_{14}$=$C_1$-$C_2$ [°] | σ $C_{14}$-$C_1$-$C_2$-$C_3$ [°] | $R_2$ $C_5$-$O_4$ [Å] | $R_D$ $C_1$-$C_{14}$ [Å] | $R_S$ $C_1$-$C_2$ [Å] | $R_E$ $C_2$-$C_3$ [Å] | $B_F$-N [°] | BB [°] | $E_a$ [eV] |
|---|---|---|---|---|---|---|---|---|---|---|
| **CF** | 1.459 | 20.1 | 3.8 | 1.371 | 1.461 | 1.360 | 1.514 | 78.4 | 82.2 | 0.00 |
| **$TS_1$** | 2.100 | 22.8 | 27.7 | 1.269 | 1.415 | 1.405 | 1.407 | 84.0 | 67.0 | 1.08 |
| **TC-d** | 2.779 | 17.7 | 45.0 | 1.239 | 1.388 | 1.446 | 1.380 | 69.3 | 70.5 | 0.84 |
| **$TS_2$** | 3.098 | 2.6 | 90.0 | 1.235 | 1.371 | 1.479 | 1.363 | 82.8 | 82.3 | 1.04 |
| **TC-u** | 4.165 | 2.6 | 173.5 | 1.239 | 1.386 | 1.437 | 1.362 | 63.7 | 70.3 | 0.59 |
| **$TS_{3\text{-}1}$** | 4.740 | -90.0 | -157.0 | 1.236 | 1.418 | 1.429 | 1.392 | 80.2 | 66.3 | 1.874 |
| **$TS_{3\text{-}2}$** | 4.739 | 90.0 | 156.9 | 1.236 | 1.418 | 1.429 | 1.392 | 80.2 | 66.3 | 1.874 |
| **$TT\text{-}u_1$** | 5.064 | 165.1 | 172.1 | 1.234 | 1.382 | 1.440 | 1.382 | 50.6 | 68.5 | 0.62 |
| **$TT\text{-}u_2$** | 5.046 | -166.2 | 179.7 | 1.234 | 1.383 | 1.439 | 1.382 | 50.1 | 73.8 | 0.69 |
| **TT-d** | 5.219 | 162.0 | -43.3 | 1.233 | 1.375 | 1.461 | 1.377 | 12.8 | 72.7 | 0.64 |
| **AP** | 3.413 | 34.3 | 30.3 | 1.360 | 1.478 | 1.334 | 1.339 | 73.6 | 62.6 | 1.01 |
| **$TS_4$** | 3.615 | 9.2 | 161.5 | 1.284 | 1.413 | 1.405 | 1.384 | 48.3 | 59.9 | 1.677 |

**Table S5.** Comparison of the geometric parameters (bond lengths, in Å, dihedral angles), adiabatic energies ($E_a$, in eV) for the excited state ($S_1$) geometries optimized at the **ADC(2)/cc-pVDZ** level of theory. Conical intersection **CI($S_1$/$S_0$)** geometry designated as $CI_1^{MPE}$ - the intersection of the excited-state MPE profile with the ground electronic state, $S_0$ at the **ADC(2)($S_1$)/MP2($S_0$)/cc-pVDZ** theory level.

| $S_1$-state form or CI | R $C_3$-$O_4$ [Å] | δ $C_5$-$C_{14}$=$C_1$-$C_2$ [°] | σ $C_{14}$-$C_1$-$C_2$-$C_3$ [°] | τ $C_6$-$C_5$-$C_{14}$-$C_1$ [°] | $R_2$ $C_5$-$O_4$ [Å] | $R_D$ $C_1$-$C_{14}$ [Å] | $R_S$ $C_1$-$C_2$ [Å] | $R_E$ $C_2$-$C_3$ [Å] | $B_F$-N [°] | BB [°] | $E_a$ [eV] |
|---|---|---|---|---|---|---|---|---|---|---|---|
| **TC-d** | 2.600 | 45.1 | 7.6 | 176.9 | 1.276 | 1.479 | 1.362 | 1.471 | 27.3 | 59.5 | 1.74 |
| **$CI_1$** | 2.200 | 28.8 | 17.4 | 178.4 | 1.282 | 1.447 | 1.384 | 1.450 | 42.4 | 59.5 | 1.91 |
| **TT-u** | 4.433 | -91.3 | 170.0 | 180.0 | 1.266 | 1.474 | 1.366 | 1.445 | 58.0 | 59.7 | 1.85 |
| **TC-u** | 3.921 | 22.5 | -174.8 | 174.2 | 1.399 | 1.478 | 1.371 | 1.440 | 45.0 | 58.7 | 2.14 |

**Table S6**. Theoretical predictions for the spectral position ($cm^{-1}$) of vibrational C=O stretching mode of **TC-u**, **TC-d**, **TT-u** and **TT-d** isomers (at **B3LYP/6-311++G(3df,3pd)** level of theory with polarizable continuum model for cyclohexane). Scaling factor 0.98385 is an average of factors for **TC-u** and **TT-u**, (see Fig. S2).

| form | ν, $cm^{-1}$ |
|---|---|
| **TC-u** | 1641.36 |
| **TC-d** | 1653.83 |
| **TT-u** | 1655.47 |
| **TT-d** | 1662.26 |

**Table S7.** Comparison of the geometric parameters (bond lengths, in Å, dihedral angles), adiabatic energies ($E_a$, in eV) for the conical intersection **CI($S_1$/$S_0$)** geometries designated as CI – obtained by means of the geometry optimization of the minimum energy crossing point (CI) using program[7, 8] at the **ADC(2)($S_1$)/MP2($S_0$)/cc-pVDZ** theory level.

| CI | $R_1$ $C_3$-$O_4$ [Å] | δ $C_5$-$C_{14}$-$C_1$-$C_2$ [°] | σ $C_{14}$-$C_1$-$C_2$-$C_3$ [°] | τ $C_6$-$C_5$-$C_{14}$-$C_1$ [°] | $R_2$ $C_5$-$O_4$ [Å] | $R_D$ $C_1$-$C_{14}$ [Å] | $R_S$ $C_1$-$C_2$ [Å] | $R_E$ $C_2$-$C_3$ [Å] | $B_F$-N [°] | BB [°] | $E_a$ [eV] |
|---|---|---|---|---|---|---|---|---|---|---|---|
| **$CI_1$** | 2.389 | 35.2 | 16.7 | 172.5 | 1.288 | 1.457 | 1.376 | 1.450 | 86.9 | 60.6 | 1.84 |
| **$CI_2$** | 3.924 | 22.9 | 174.7 | 174.2 | 1.400 | 1.479 | 1.370 | 1.441 | 17.1 | 58.8 | 2.14 |
| **$CI_3$** | 4.527 | -115.9 | 170.1 | 178.7 | 1.278 | 1.481 | 1.366 | 1.446 | 30.3 | 57.7 | 2.21 |

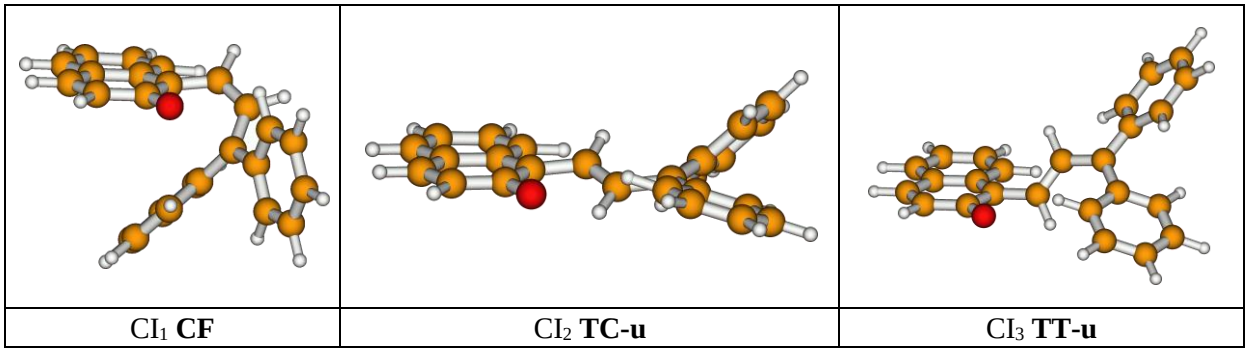

$CI_1$ **CF** | $CI_2$ **TC-u** | $CI_3$ **TT-u**

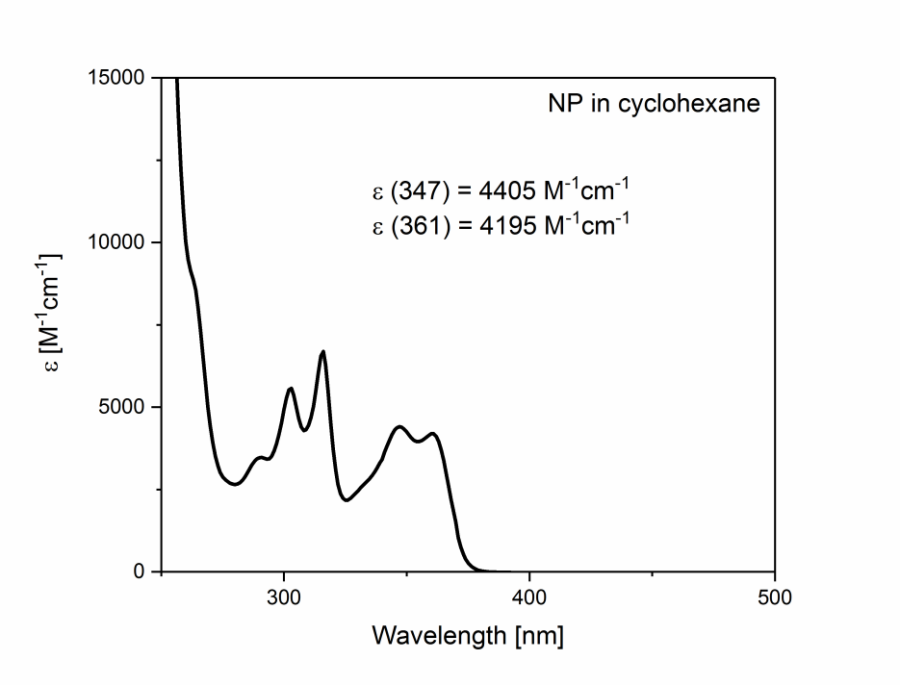


**Figure S1.** Stationary UV-vis absorption spectrum of **NP** in cyclohexane.

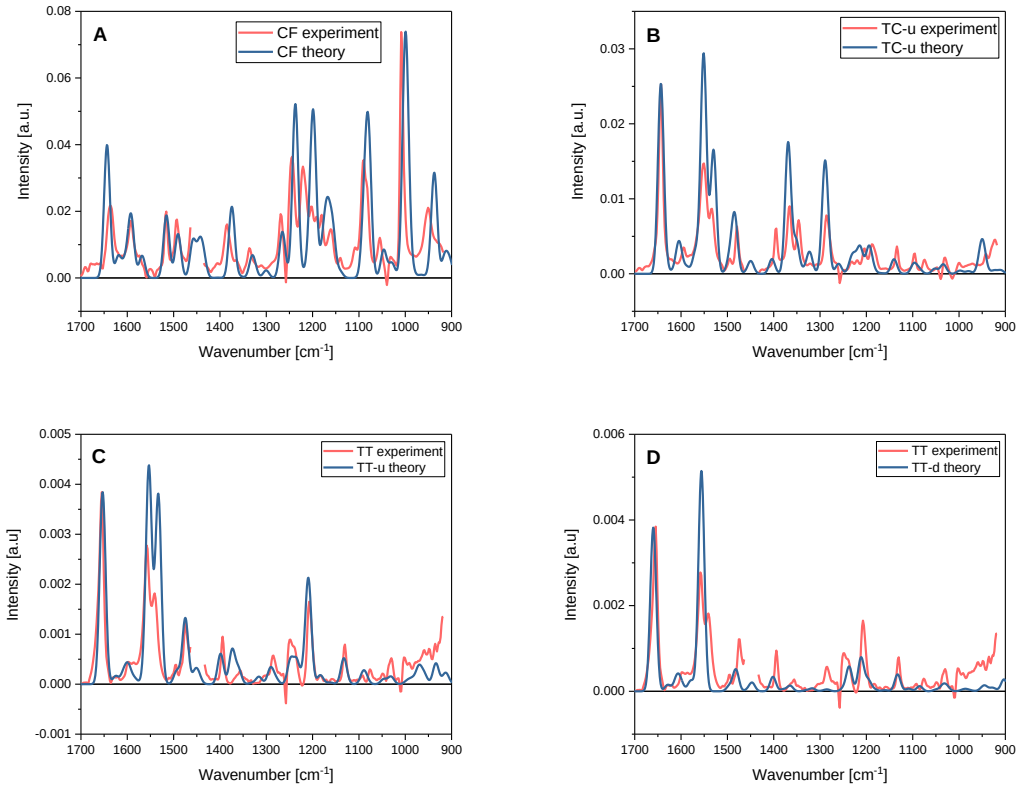


**Figure S2.** Calculated vibrational mid-IR spectra for the optimized structures of **CF** (A), **TC-u** (B), **TT-u** (C) and **TT-d** (D) at the **B3LYP/6-311++G(3df,3pd)** level of theory with polarizable continuum model (PCM) for cyclohexane. Parameters used: $\Delta\tilde{\nu}$ = 15 cm$^{-1}$ (FWHM), scaling factors: 0.9795 (**CF**), 0.9852 (**TC-u**) and 0.9825 (**TT-u** and **TT-d**). Theoretical predictions are compared with experimental data obtained for photolyzed **NP** solution in cyclohexane using time-resolved FT-IR spectroscopy (data from Figure 4, solution thickness 140 μm).

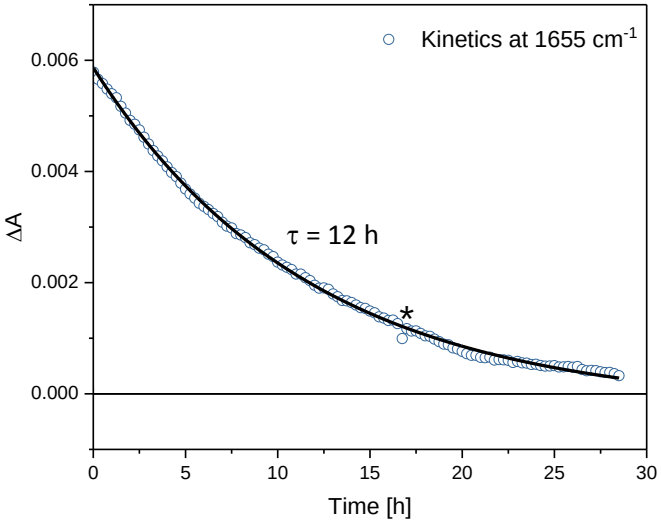


**Figure S3.** The long-lived **TT-u** population is generated upon 30 s UV irradiation of **NP** solution in cyclohexane ($2.8 \times 10^{-3}$ M, cell with 0.95 mm spacer). Decay of **TT-u** population is observed over tens of hours in the dark at T = 23°C. Time window is 1–1710 min. (*) Artefact due to filling the MCT detector with liquid nitrogen.

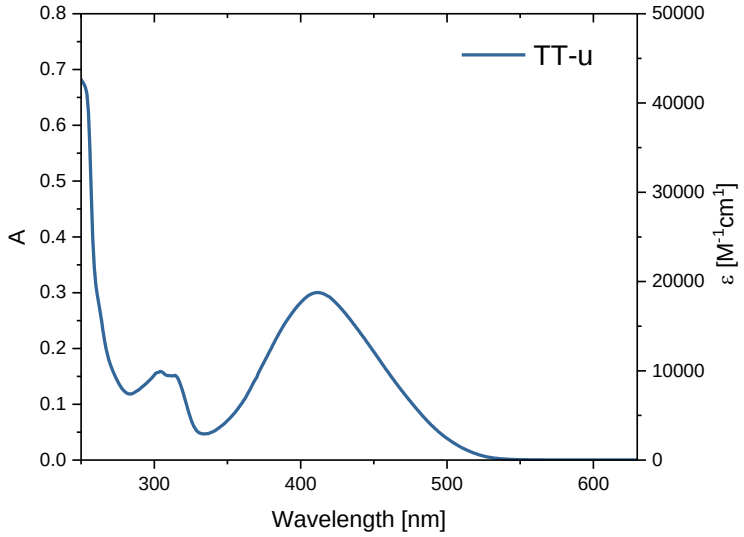


**Figure S4. TT-u** absorption spectrum calculated from stationary UV-Vis absorption data recorded with Jasco for UV-irradiated **NP** solution. **CF** contribution was removed from the spectrum using the FT-IR data to estimate the part of **CF** population converted to **TT-u** (on the basis of initial **CF** absorption signal at 1009 $cm^{-1}$ and the **CF** bleach signal at the same wavelength at long delays in the time-resolved FTIR experiment).

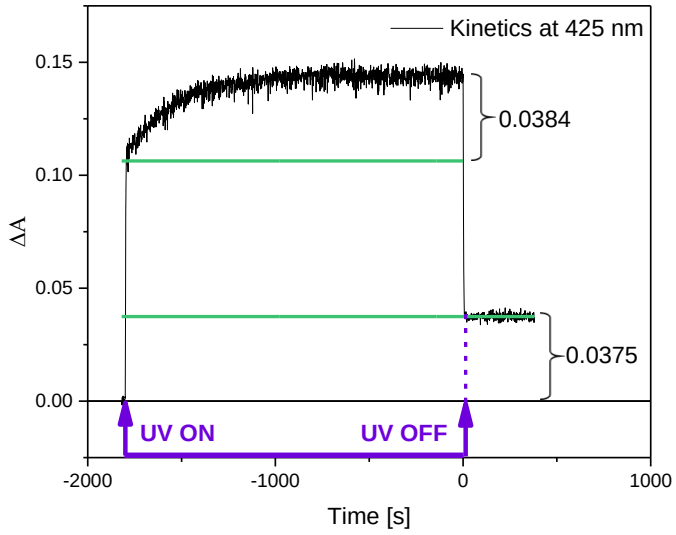


**Figure S5**. Kinetics at 425 nm for **NP** in cyclohexane upon long UV irradiation period ($3 \times 10^{-4}$ M, I = 2.7 mW/cm$^2$, $\lambda_{exc}$ = 365 nm, T = 40°C). The kinetic trace indicates that **TT-u** form (offset) is almost equal to the amplitude of the slow rising component before photostationary state is reached.

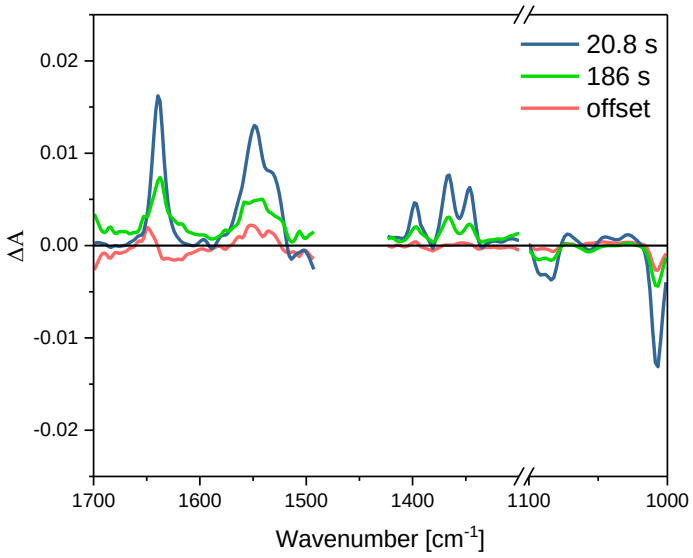


**Figure S6.** Switching off UV-irradiation of **NP** in PMMA ($\lambda_{exc}$ = 365 nm, I = 9.2 mW/cm$^2$) leads to decay of the IR absorption bands. The graph shows decay associated spectra with characteristic time constants 20.8 s and 186 s corresponding to **TC-u** form. The offset can be assigned to **TT-u** form. Negative bands reflect **CF** ground state bleaching.

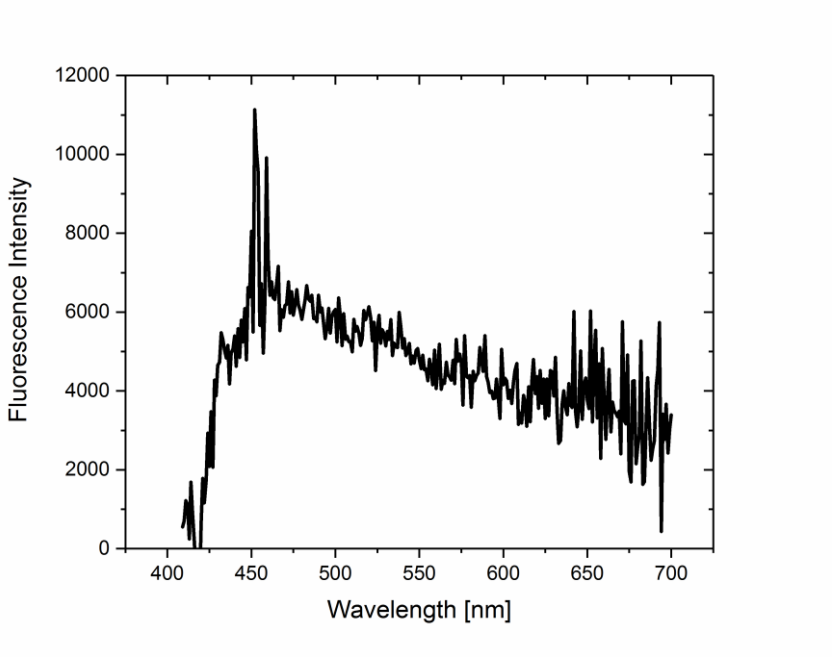


**Figure S7**. The fluorescence spectrum recorded for **TT-u** ($1 \times 10^{-5}$ M) with excitation at 400 nm. The spectrum is corrected for solvent contribution. Emission spectrum was recorded on a Horiba Jobin-Yvon-Spex Fluorolog 3-22 spectrofluorometer. Right-angle geometry was used. Three fluorescence spectra were collected with 1 nm excitation and emission slits, and 0.5 s integration time. Experiment was performed on 3.5 mL solution samples contained in a quartz cell (1 cm ×1 cm ). A very low fluorescence quantum yield $\Phi_f \approx 7 \times 10^{-5}$ is determined using 9,10-diphenylanthracene in cyclohexane as a standard, $\Phi_f = 0.97$.[9]

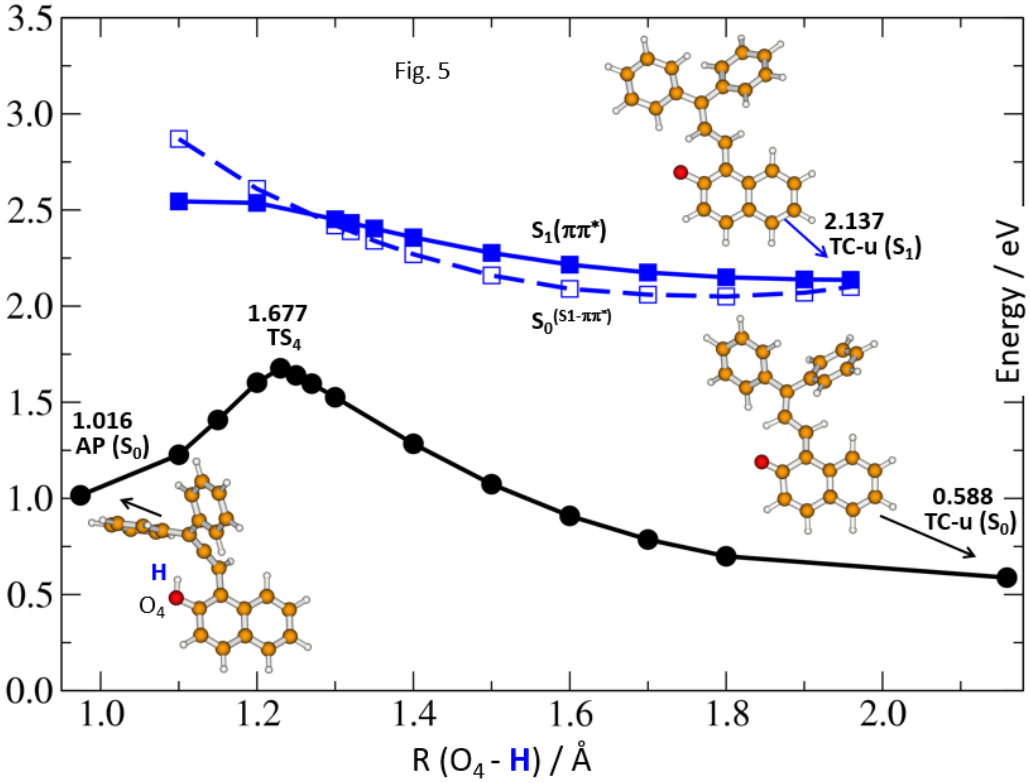


**Figure S8.** Photoinduced ESIPT upon **TC-u** photoexcitation leading to **AP** form.

**Important geometries in the Cartesian Coordinates format**

Geometry of the conical intersection **$CI_1$** optimized by relaxed scan at the **ADC(2)($S_1$)/MP2($S_0$)/cc-pVDZ** theory level.

$E_a$ = 1.84 eV

| | | | |
|---|---|---|---|
| C | -3.28277 | -1.39800 | -0.95957 |
| C | -4.63635 | -1.57624 | -0.68759 |
| C | -5.40598 | -0.49554 | -0.18310 |
| C | -4.81100 | 0.74235 | 0.04490 |
| C | -2.79635 | 2.20596 | 0.03314 |
| C | -1.44534 | 2.37291 | -0.18337 |
| C | -0.61887 | 1.31968 | -0.73029 |
| C | -1.25642 | 0.05806 | -1.05349 |
| C | -2.64926 | -0.13382 | -0.76603 |
| C | -3.43083 | 0.94614 | -0.22939 |
| H | -2.68602 | -2.24148 | -1.32246 |
| H | -5.10312 | -2.55397 | -0.84680 |
| H | -6.46953 | -0.63963 | 0.03537 |
| H | -5.39766 | 1.57519 | 0.44995 |
| H | -3.39781 | 3.02606 | 0.44393 |
| H | -0.94450 | 3.32151 | 0.03824 |
| O | 0.64033 | 1.52644 | -0.90164 |
| C | 1.56473 | -0.61258 | -0.37288 |
| C | 0.87034 | -1.13106 | -1.53480 |
| C | -0.47526 | -0.95103 | -1.75762 |
| H | -0.95555 | -1.47344 | -2.59686 |
| H | 1.46115 | -1.70427 | -2.26229 |
| C | 0.90644 | -0.56622 | 0.93602 |
| C | -0.11617 | -1.48658 | 1.28243 |
| C | -0.77426 | -1.38814 | 2.51689 |
| C | -0.43029 | -0.37482 | 3.42967 |
| C | 0.58997 | 0.53785 | 3.09776 |
| C | 1.25934 | 0.44365 | 1.87068 |
| H | 2.01536 | 1.18324 | 1.58896 |
| H | -0.37883 | -2.28251 | 0.57812 |
| H | -1.56074 | -2.10837 | 2.76807 |
| H | -0.95296 | -0.29434 | 4.38881 |
| H | 0.85777 | 1.33612 | 3.79890 |
| C | 2.99116 | -0.30726 | -0.49361 |
| C | 3.48554 | 0.26642 | -1.69209 |
| C | 4.85422 | 0.52939 | -1.84055 |
| C | 5.75561 | 0.22544 | -0.80282 |
| C | 5.27185 | -0.33976 | 0.39126 |
| C | 3.90316 | -0.60020 | 0.55300 |
| H | 3.53214 | -1.06112 | 1.47443 |
| H | 2.77146 | 0.54675 | -2.47357 |
| H | 5.22091 | 0.98662 | -2.76622 |
| H | 6.82460 | 0.43163 | -0.92195 |
| H | 5.96805 | -0.58382 | 1.20128 |

Geometry of the conical intersection **$CI_2$** optimized by relaxed scan at the **ADC(2)($S_1$)/MP2($S_0$)/cc-pVDZ** theory level.

$E_a$ = 2.14 eV

| | | | |
|---|---|---|---|
| C | -2.75611 | -2.35930 | -0.10429 |
| C | -3.91878 | -3.11380 | -0.10672 |
| C | -3.86509 | -4.53182 | 0.05233 |
| C | -2.64494 | -5.16402 | 0.20301 |
| C | -0.16970 | -5.04381 | 0.34362 |
| C | 1.01084 | -4.29336 | 0.31599 |
| C | 0.93948 | -2.89331 | 0.19599 |
| C | -0.26354 | -2.20575 | 0.09415 |
| C | -1.47316 | -2.97511 | 0.07135 |
| C | -1.42448 | -4.41039 | 0.20970 |
| H | -4.88655 | -2.61941 | -0.24339 |
| H | -2.81686 | -1.27694 | -0.25311 |
| H | -4.79184 | -5.11514 | 0.04714 |
| H | -2.58693 | -6.25330 | 0.31292 |
| H | -0.11667 | -6.13407 | 0.44735 |
| H | 1.99022 | -4.77595 | 0.40309 |
| O | 2.17970 | -2.24427 | 0.18361 |
| C | -0.28526 | -0.72676 | 0.09990 |
| C | 0.80708 | 0.02129 | -0.25268 |
| H | -1.17046 | -0.23493 | 0.52124 |
| H | 1.70036 | -0.51426 | -0.62062 |
| C | 0.92180 | 1.45533 | -0.17804 |
| C | -0.27561 | 2.29868 | -0.09219 |
| C | 2.25670 | 2.05075 | -0.16954 |
| C | -0.30770 | 3.42876 | 0.76726 |
| C | -1.46215 | 4.21886 | 0.86778 |
| C | -2.60397 | 3.91373 | 0.10424 |
| C | -2.58159 | 2.80423 | -0.76105 |
| C | -1.43602 | 2.00068 | -0.85578 |
| H | 0.57252 | 3.65983 | 1.37688 |
| H | -1.47329 | 5.07606 | 1.55003 |
| H | -3.50154 | 4.53656 | 0.18041 |
| H | -3.46042 | 2.56839 | -1.37144 |
| H | -1.41097 | 1.15286 | -1.54881 |
| C | 2.48132 | 3.36725 | -0.65727 |
| C | 3.77248 | 3.91358 | -0.66670 |
| C | 4.86755 | 3.17294 | -0.18547 |
| C | 4.65700 | 1.86906 | 0.30271 |
| C | 3.37165 | 1.31246 | 0.31538 |
| H | 1.63953 | 3.93992 | -1.06027 |
| H | 3.92750 | 4.92453 | -1.05980 |
| H | 5.87346 | 3.60578 | -0.19120 |
| H | 5.50067 | 1.28721 | 0.69007 |
| H | 3.21380 | 0.30698 | 0.72222 |

Geometry of the conical intersection **$CI_3$** optimized by relaxed scan at the **ADC(2)($S_1$)/MP2($S_0$)/cc-pVDZ** theory level.

$E_a$ = 2.21 eV

| | | | |
|---|---|---|---|
| C | -1.36084 | -2.71731 | -1.07577 |
| C | -2.35093 | -3.63390 | -1.40584 |
| C | -2.22320 | -4.99563 | -1.01459 |
| C | -1.09829 | -5.42098 | -0.31318 |
| C | 1.10641 | -4.93353 | 0.74573 |
| C | 2.10654 | -4.04278 | 1.07742 |
| C | 2.02163 | -2.63368 | 0.72718 |
| C | 0.83946 | -2.21906 | 0.01738 |
| C | -0.19698 | -3.11912 | -0.34170 |
| C | -0.06580 | -4.50830 | 0.03458 |
| H | -3.23123 | -3.30905 | -1.97103 |
| H | -1.44877 | -1.67193 | -1.39325 |
| H | -3.01005 | -5.71218 | -1.27352 |
| H | -0.99180 | -6.47296 | -0.02253 |
| H | 1.18962 | -5.99054 | 1.02864 |
| H | 2.99660 | -4.36489 | 1.63017 |
| O | 2.92530 | -1.78778 | 1.04513 |
| C | 0.82282 | -0.76660 | -0.27167 |
| C | -0.10203 | 0.09385 | 0.24799 |
| H | -0.95159 | -0.32323 | 0.80690 |
| C | -0.01648 | 1.53341 | 0.14517 |
| C | 1.26289 | 2.17948 | -0.13906 |
| C | -1.21314 | 2.33371 | 0.39211 |
| C | 1.30472 | 3.36824 | -0.92001 |
| C | 2.52947 | 3.98066 | -1.21438 |
| C | 3.73145 | 3.43967 | -0.71927 |
| C | 3.70075 | 2.27009 | 0.06243 |
| C | 2.48450 | 1.63543 | 0.35189 |
| H | 0.37276 | 3.77479 | -1.32669 |
| H | 2.54937 | 4.88142 | -1.83728 |
| H | 4.68653 | 3.92579 | -0.94545 |
| H | 4.63101 | 1.84465 | 0.45341 |
| H | 2.47814 | 0.72275 | 0.95958 |
| C | -1.12496 | 3.62766 | 0.97441 |
| C | -2.28553 | 4.36695 | 1.23986 |
| C | -3.55272 | 3.84523 | 0.91953 |
| C | -3.65257 | 2.56662 | 0.33923 |
| C | -2.49934 | 1.81366 | 0.08298 |
| H | -0.14312 | 4.02294 | 1.25387 |
| H | -2.20277 | 5.35424 | 1.70682 |
| H | -4.45631 | 4.42916 | 1.12391 |
| H | -4.63533 | 2.15811 | 0.08071 |
| H | -2.58214 | 0.82860 | -0.38957 |
| H | 1.65593 | -0.37369 | -0.87224 |

## Calculation of quantum yields of CF→TC and TC→TT photoconversion reactions

To extract quantum yields of **CF→TC**, **TC→TT** and **TT→TC** photoconversion, we used NDSolve function in Mathematica software, which allowed to solve numerically set of differential equations, which describe observed reactions.[10] Kinetics recorded using Jasco spectrophotometer were fitted by functions obtained iteratively from NDSolve. Rate constants of thermal reactions were determined separately by fitting decay kinetics measured after switching off UV irradiation. Photon flux and initial absorbance were experimentally determined and kept as constraints. The only parameters in fitting procedure were quantum yields. Quantum yields of **CF→TC**, **TC→TT** photoconversion were obtained by fitting of kinetics measured at 450 nm during irradiation at 365 nm. Quantum yield of **TT→TC** photoconversion was obtained by fitting of kinetics measured at 450 nm during irradiation at 408 nm (laser LED).

Incident photon flux $I_0$ was determined by potassium ferrioxalate actinometer. Potassium ferrioxalate crystals were obtained by reaction of potassium oxalate with iron (III) chloride, and triple recrystallization.[11] 0.012 M potassium ferrioxalate solution and 0.1% phenanthroline solution were prepared in appropriate buffers accordingly to Handbook of photochemistry.[12] 1.5 mL actinometer solution in 10 × 10 $mm^2$ cuvette (the same type of cuvette and amount of sample was used for naphthopyrans) was irradiated for 10 s, then 250 μL of phenanthroline solution was added and absorption spectrum was measured immediately (experimental conditions were selected to obtain A(510 nm) between 0.2 and 0.3). Before calculation of photon flux, spectrum obtained for reference (not irradiated) actinometer was subtracted. For 365 nm and 408 nm irradiation 1.22 and 1.15 quantum yields were used, respectively.

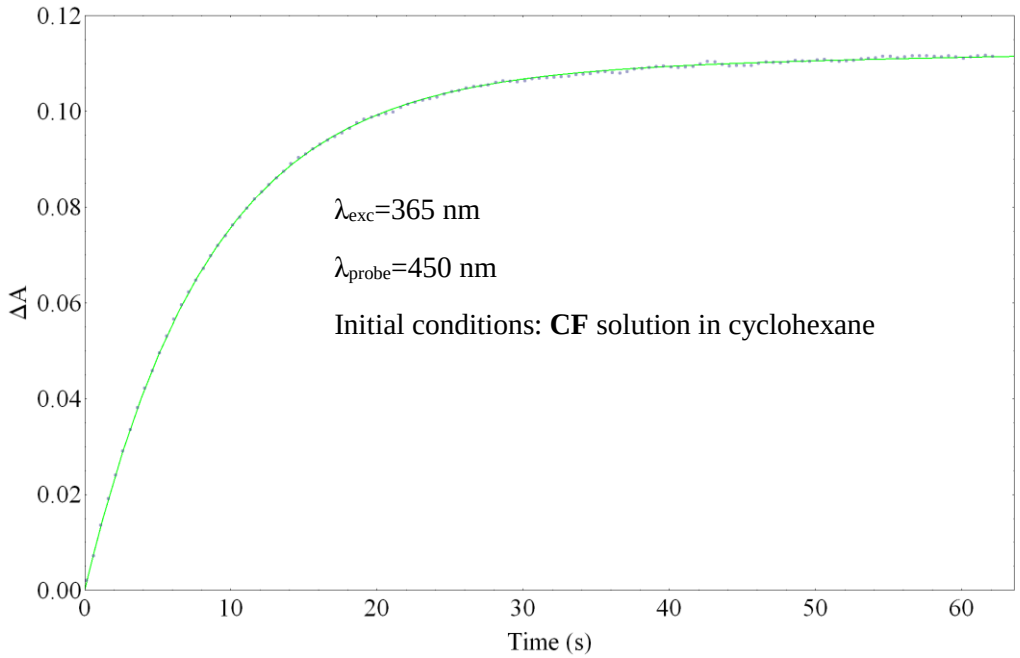


**Figure S9**. **CF** solution in cyclohexane in 1 cm × 1 cm cell with stirring within thermostatic holder (T = 22°C). Switching on UV irradiation (365 nm) causes the increase in absorbance signal at 450 nm.

Following constraints were used:

$\varepsilon_{CF}[365] = 3389\ L\ mol^{-1}\ cm^{-1}$
$\varepsilon_{CF}[450] = 0\ L\ mol^{-1}\ cm^{-1}$
$\varepsilon_{TC}[365] = \varepsilon_{CF}[365]$
$\varepsilon_{TC}[450] = 16154\ L\ mol^{-1}\ cm^{-1}$
$\varepsilon_{TT}[365] = \varepsilon_{CF}[365]$
$\varepsilon_{TT}[450] = 11850\ L\ mol^{-1}\ cm^{-1}$
$I_0 = 0.00000153\ mol\ L^{-1}\ s^{-1}$ (incident photon flux)
$k = 0.1132\ s^{-1}$ (thermal TC→CF reaction)
$A_0[365] = 0.53$ (initial CF absorbance at excitation wavelength)

Differential equations to solve:

$$\mathrm{CF}'[t] = -\phi_1 F[t] I_0 \epsilon_{\mathrm{CF}}[365] l_i \mathrm{CF}[t] + \mathrm{TC}[t]\mathrm{k1},$$

$$\mathrm{TC}'[t] = \phi_1 F[t] I_0 \epsilon_{\mathrm{CF}}[365] l_i \mathrm{CF}[t] - \phi_2 F[t] I_0 \epsilon_{\mathrm{TC}}[365] l_i \mathrm{TC}[t] - \mathrm{TC}[t]\ \mathrm{k},$$

$$\mathrm{TT}'[t] = \phi_2 F[t] I_0 \epsilon_{\mathrm{TC}}[365] l_i \mathrm{TC}[t],$$

where CF[t], TC[t], TT[t] are concentrations, $l_i$ is irradiation optical path length, $F[\mathrm{t}] = \frac{1-\mathrm{Exp}[-2.3 A_T[t]]}{A_T[t]}$ is photokinetic factor, where $A_T[t]$ is total absorbance at probing wavelength.

Obtained quantum yields:

$\phi_1 = 0.745$ (**CF→TC**)

$\phi_2 = 0.1$ (**TC→TT**)

## Calculation of quantum yield of TT→TC photoconversion reaction

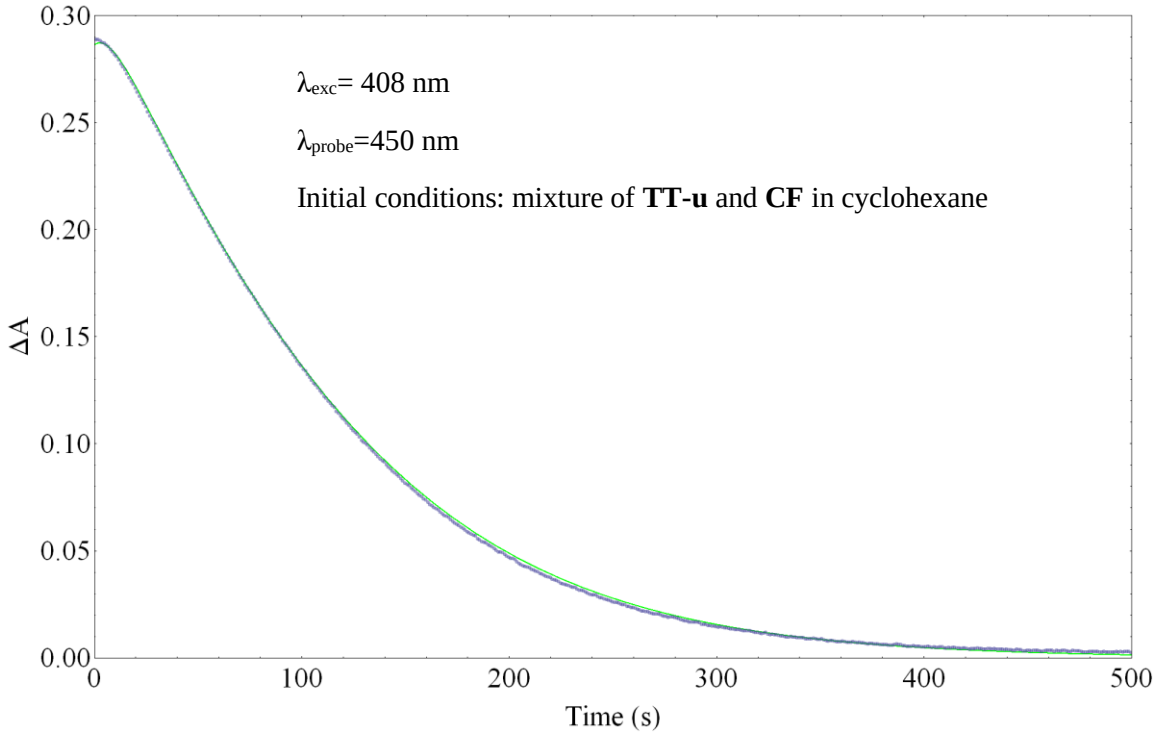


**Figure S10**. Mixture of **TT-u** and **CF** in cyclohexane in 1 cm × 1 cm cell with stirring within thermostatic holder (T = 22°C). Switching on blue irradiation (408 nm) causes the decrease in absorbance signal at 450 nm.

Following constraints were used:

$\varepsilon_{TT}[408] = 18216\ L\ mol^{-1}\ cm^{-1}$
$\varepsilon_{TT}[450] = 11850\ L\ mol^{-1}\ cm^{-1}$
$\varepsilon_{TC}[408] = 16200\ L\ mol^{-1}\ cm^{-1}$
$\varepsilon_{TC}[450] = 16154\ L\ mol^{-1}\ cm^{-1}$
$\varepsilon_{CF}[408] = 0\ L\ mol^{-1}\ cm^{-1}$
$\varepsilon_{CF}[450] = 0\ L\ mol^{-1}\ cm^{-1}$
$I_0 = 0.00000269\ mol\ L^{-1}\ s^{-1}$ (incident photon flux)
$k = 0.1132\ s^{-1}$ (thermal TC→CF reaction)
$A_0[408] = 0.44$ (initial absorbance at excitation wavelength)

Differential equations to solve:

$$\mathrm{TT}'[t] = -\phi F[t] I_0 \epsilon_{\mathrm{TT}}[408] l_i \mathrm{TT}[t]$$

$$\mathrm{TC}'[t] = \phi F[t] I_0 \epsilon_{\mathrm{TT}}[408] l_i \mathrm{TT}[t] - \mathrm{TC}[t]\,\mathrm{k}$$

$$\mathrm{CF}'[t] = \mathrm{TC}[t]\,\mathrm{k},$$

where CF[t], TC[t], TT[t] are concentrations, $l_i$ is irradiation optical path length,
$F[\mathrm{t}] = \frac{1-\mathrm{Exp}[-2.3 A_T[t]]}{A_T[t]}$ is photokinetic factor, where $A_T[t]$ is total absorbance at probing wavelength.

Obtained quantum yield

$\phi = 0.107$ (**TT→TC**)

## References


1. I. Schapiro, O. Weingart and V. Buss, *J. Am. Chem. Soc.*, 2009, **131**, 16-17.
2. A. Warshel, *Nature*, 1976, **260**, 679-683.
3. H. Böhnke, J. Bahrenburg, X. Ma, K. Röttger, C. Näther, M. F. Rode, A. L. Sobolewski and F. Temps, *Phys. Chem. Chem. Phys.*, 2018, **20**, 2646-2655.
4. A. Dreuw and M. Wormit, *WIREs Comput. Mol. Sci.*, 2015, **5**, 82-95.
5. C. Hättig and K. Hald, *Phys. Chem. Chem. Phys.*, 2002, **4**, 2111-2118.
6. M. F. Rode and A. L. Sobolewski, *Chem. Phys.*, 2008, **347**, 413-421.
7. B. G. Levine, J. D. Coe and T. J. Martínez, *J. Phys. Chem. B*, 2008, **112**, 405-413.
8. R. Szabla, R. W. Góra and J. Šponer, *Phys. Chem. Chem. Phys.*, 2016, **18**, 20208-20218.
9. K. Suzuki, A. Kobayashi, S. Kaneko, K. Takehira, T. Yoshihara, H. Ishida, Y. Shiina, S. Oishi and S. Tobita, *Phys. Chem. Chem. Phys.*, 2009, **11**, 9850-9860.
10. J. C. Crano and R. Guglielmetti, *Organic photochromic and thermochromic compounds: Physicochemical studies, biological applications, and thermochromism*, Plenum Press, New York, 1999.
11. H. J. Kuhn, S. E. Braslavsky and R. Schmidt, *Pure Appl. Chem.*, 2004, **76**, 2105−2146.
12. M. Montalti, A. Credi, L. Prodi and M. Gandolfi, *Handbook of Photochemistry*, CRC Press, Boca Raton, 2006.